AD-A173 539 COLLISIONLESS COUPLING IN THE AMPTE (ACTIVE MAGNETOSPHERIC PARTICLE TRACE..(U) NAVAL RESEARCH LAB WASHINGTON DC K PAPADOPOULOS ET AL. 29 SEP 86

1/1

UNCLASSIFIED NRL-MR-5835 F/G 4/1 NL

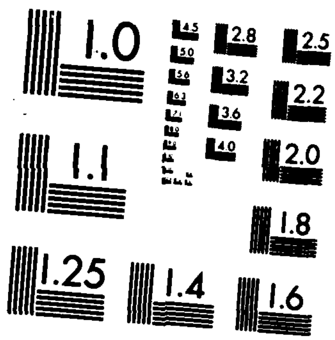

MICROCOPY RESOLUTION TEST CHART
NATIONAL BUREAU OF STANDARDS-1963-A

Naval Research Laboratory

Washington, DC 20375-5000 NRL Memorandum Report 5835 September 29, 1986

(2)

AD-A173 539

Collisionless Coupling in the AMPTE Artificial Comet

K. PAPADOPOULOS

Science Applications International Corporation
McLean, Virginia 22102

J. D. HUBA

Geophysical and Plasma Dynamics Branch
Plasma Physics Division

A. T. Y. LUI

Applied Physics Laboratory
Johns Hopkins University
Laurel, Maryland 20707

This research was partially sponsored by the Office of Naval Research and the Defense Nuclear Agency under Subtask S99QMXBC, work unit 00146 and work unit title "Weapons Phenomenology and Code Development."

SECURITY CLASSIFICATION OF THIS PAGE

REPORT DOCUMENTATION PAGE

1a REPORT SECURITY CLASSIFICATION UNCLASSIFIED	1b RESTRICTIVE MARKINGS
2a SECURITY CLASSIFICATION AUTHORITY	3 DISTRIBUTION/AVAILABILITY OF REPORT Approved for public release; distribution unlimited.
2b DECLASSIFICATION/DOWNGRADING SCHEDULE	
4 PERFORMING ORGANIZATION REPORT NUMBER(S) NRL Memorandum Report 5835	5 MONITORING ORGANIZATION REPORT NUMBER(S)
6a NAME OF PERFORMING ORGANIZATION Naval Research Laboratory / 6b OFFICE SYMBOL (If applicable) Code 4780	7a NAME OF MONITORING ORGANIZATION
6c ADDRESS (City, State, and ZIP Code) Washington, DC 20375-5000	7b ADDRESS (City, State, and ZIP Code)
8a NAME OF FUNDING/SPONSORING ORGANIZATION (See Page ii) / 8b OFFICE SYMBOL (If applicable)	9 PROCUREMENT INSTRUMENT IDENTIFICATION NUMBER
8c ADDRESS (City, State, and ZIP Code) Arlington, VA 22217 (ONR) Washington, DC 20305 (DNA)	10 SOURCE OF FUNDING NUMBERS

PROGRAM ELEMENT NO.	PROJECT NO.	TASK NO	WORK UNIT ACCESSION NO.
61153N	RR033-02-44	00152 S99QMXBC	404377-85

11 TITLE (Include Security Classification)

Collisionless Coupling in the AMPTE Artificial Comet

12 PERSONAL AUTHOR(S)

Papadopoulos, K., Huba, J. D., and Lui, A. T. Y.

13a TYPE OF REPORT	13b TIME COVERED	14 DATE OF REPORT (Year, Month, Day)	15 PAGE COUNT
Interim	FROM ______ TO ______	29 September 1986	37

16 SUPPLEMENTARY NOTATION

(See Page ii)

17 COSATI CODES			18 SUBJECT TERMS (Continue on reverse if necessary and identify by block number)
FIELD	GROUP	SUB-GROUP	Early time coupling; Ion/ion interactions Magnetized ion instability, AMPTE release.

19 ABSTRACT (Continue on reverse if necessary and identify by block number)

Analysis of previously reported observations of the solar wind/barium interaction associated with the AMPTE artificial comet release of Dec. 27, 1984 is presented. Based on these results we argue that the solar wind couples momentum (and energy) to the barium ions through both laminar and turbulent processes. The laminar forces acting on the particles are the laminar electric and magnetic fields; the turbulent forces are associated with the intense electrostatic wave activity. This wave activity is shown to be caused by a cross-field solar wind proton/barium ion streaming instability. The observed wave frequencies and saturated amplitudes are consistent with our theoretical analysis.

20 DISTRIBUTION/AVAILABILITY OF ABSTRACT ☒ UNCLASSIFIED/UNLIMITED ☐ SAME AS RPT ☐ DTIC USERS	21 ABSTRACT SECURITY CLASSIFICATION UNCLASSIFIED	
22a NAME OF RESPONSIBLE INDIVIDUAL J. D. HUBA	22b TELEPHONE (Include Area Code) 202-767-3630	22c OFFICE SYMBOL Code 4780

DD FORM 1473, 84 MAR — 83 APR edition may be used until exhausted. All other editions are obsolete.

SECURITY CLASSIFICATION OF THIS PAGE

8a. NAME OF FUNDING/SPONSORING ORGANIZATION

Office of Naval Research
Defense Nuclear Agency

16. SUPPLEMENTARY NOTATION

This research was partially sponsored by the Office of Naval Research and the Defense Nuclear Agency under Subtask S99QMXBC, work unit 00146 and work unit title "Weapons Phenomenology and Code Development."

CONTENTS

COLLISIONLESS COUPLING IN THE AMPTE ARTIFICIAL COMET

I. INTRODUCTION

The in situ measurements of the plasma parameters from the AMPTE (Active Magnetospheric Particle Tracer Explorers) artificial comet releases (Valenzuela et al., 1986; Haerendel et al., 1986) in the solar wind provide us with a unique set of data to test the available theories on the subject of collisionless coupling of magnetized plasma streams under high Mach number conditions ($M_A >> 1$) (Haerendel et al., 1986). The subject is very opportune since it is the controlling factor that determines the momentum coupling process occurring in the interaction of the solar wind with the cometary plasma generated by the ionization of the neutral coma. The overall comet structure, the applicability of MHD or kinetic models, the presence or absence of a cometary shock and the type of the resulting ionopause (Mendis and Houpis, 1982; Ip and Axford, 1982; Fedder et al., 1986; Sagdeev et al., 1986) depends critically on the wave-particle processes producing the momentum coupling, the thermalization, and the isotropization in the interaction. It is the purpose of the present note to compare the AMPTE in situ observations of the plasma parameters and wave signatures (Gurnett et al., 1985; Haerendel et al., 1986) with the theoretical concepts currently applied to the high Mach number interaction problem. In the next section we present a brief description of the experiment as well as the relevant data. Section III reviews the theoretical models for coupling. Section IV compares the AMPTE data with the observations.

II. OBSERVATIONAL RESULTS

During the artificial comet experiment on Dec 27, 1984 two canisters of barium were released from the IRM (Ion Release Module) spacecraft. The release was on the morning side of the earth at a geocentric radial distance of roughly 17 earth radii. The canisters were exploded simultaneously at a distance ~ 1 km from the spacecraft at 1232 UT. The explosion

Manuscript approved June 5, 1986.

produced an expanding barium cloud which was rapidly ionized by solar UV (τ_i = 28 sec where τ_i is the photoionization time). The interaction of the solar wind, which was flowing at ~ 550 km/sec, with the ionized barium cloud was recorded by the IRM instruments inside the cloud and the magnetic cavity that was created. The UKS spacecraft, located ~ 170 km away, was outside the magnetic cavity and measured magnetic disturbances and particle fluxes generated by the interaction. A schematic of the spacecraft positions and the magnetic field structure is shown in Fig. 1. We comment that in addition to the in situ observations made by the IRM and UKS spacecraft, ground based and airborne optical data were also obtained during the release. Such data provides important information on the macroscopic behavior of the solar wind - barium interaction. However, for the purposes of the present study this data is not used since we are concerned with the detailed evolution of plasma and field quantities which is not provided by optical data.

We present a set of plasma and field measurements which highlight the dynamic interaction of the solar wind and the barium cloud in Figs. 2-4. In Fig. 2 we show measurements of the electron density from 15 eV to 30 eV [n_e (Fig. 2a)], the flow velocity of the solar wind protons measured in the range 20 eV to 40 keV in GSE coordinates [V_{px} (Fig. 2b) and V_{pz} (Fig. 2c)], and the magnitude of the interplanetary magnetic field [B (Fig. 2d)] (Haerendel et al., 1986). We note that the magnetic field is in the y-direction and that the electron density does not include the cold electrons associated with the barium ions. The magnetic cavity generated by the barium ions is clearly seen during the time UT 12:32:02 and UT 12:33:15. Figure 3 shows the low frequency electric field measurements as a function of time and frequency (Gurnett et al., 1985), the magnitude of the magnetic field, and the barium ion density. Figure 4 displays the electric field spectrum upstream of the ion cloud at the time of maximum intensity (UT 12:34:27) (Gurnett et al., 1985). The electrostatic waves reached amplitudes in excess of 140 mV/m. Since the electron density in Fig. 2 does not include the cold elctrons, for times prior to 12:34:30 UT we will use the number density from Fig. 3, which is based upon wave emissions at the plasma frequency. For the time period 12:34:30 UT - 12:35:30 UT the values of the electron, proton, and barium densities are not well-known. Finally, for times later than 12:35:30 UT we use the data presented in Fig. 2.

On the basis of these measurements the following picture describing the spatial evolution of the coupling between the solar wind protons and the barium emerges. For times later than UT 12:36:20 the solar wind parameters correspond to the ambient conditions ($n_e \approx 2\ cm^{-3}$, $V_{px} \approx$ 550 km/sec, $T_e \approx 2 \times 10^5$ °K and $B \approx 10\ \gamma$). The interaction between the solar wind protons and the barium cloud starts at the point marked 1, which corresponds to UT 12:36:20, as seen from the initiation of the slowing down of the solar wind (Fig. 2b). During the time period UT 12:36:20 - UT 12:35:15 the initial slowing down rate is relatively weak and is accompanied by moderate wave activity (Fig. 3), density and magnetic field compression (Fig. 2a,d). There is no plasma flow in the z-direction (Fig. 2c). This time coincides with the time that the UK spacecraft records fluxes of hot electrons (> 100 eV). A much stronger slowing down rate is observed between UT 12:35:15 and UT 12:34:25, accompanied by strong electrostatic wave activity near the local proton lower hybrid frequency. For $B \approx 30 - 90\gamma$, $n_p \approx 2 - 10\ cm^{-3}$, and $n_e \approx 2 - 120\ cm^{-3}$ we note that the proton lower hybrid frequency is $f_{Hp} \approx 10 - 30$ Hz. The magnetic field, density, and the temperature continue to increase, while the value of V_{pz} remains relatively unchanged. This continues until UT 12:34:25 which is marked as 3. At this point the magnetic field has a value $B \approx 85\ \gamma$, the solar wind stream has slowed down to $V_{px} \approx 270$ km/sec, corresponding to 0.4 keV flow energy, while a broad ion distribution is observed with an equivalent temperature of 4×10^6 °K (i.e., 0.4 KeV). Notice that at this point the solar wind has lost more than 80% of its flow energy and its thermal spread is comparable to its flow speed. This corresponds to the peak of the electrostatic wave activity (see Fig. 3). The slowing down of the solar wind continues until UT 12:33:20. The magnetic field exceeds 120 γ and approaches its maximum value of 145 γ. Finally, at UT 12:33:15 we note the beginning of the magnetic cavity, the suppression of the wave activity, and the appearance of sunward flowing 0.5 KeV ions. A summary of the key parameters observed during the above times is given in Table I.

We note that there is a marked difference in the nature of the slowing down of the solar wind between the time periods UT 12:36:20 - UT 12:35:27 and UT 12:35:27 - UT 12:34:17. In the former case we point out that the low frequency electrostatic wave activity is intense and that there is little change in the z-component of the solar wind velocity. In the latter time period, the electrostatic noise has weakened considerably and there is

a substantial increase in V_{pz}. These issues will be discussed in more detail in Section IV.

III. COLLISIONLESS MOMENTUM COUPLING: THEORETICAL CONCEPTS

Prior to discussing the interpretation of the above data with respect to the physics of momentum coupling, we present a brief review of the various coupling processes. We consider the following momentum equation in the x direction for a solar wind proton (i.e., radial direction perpendicular to the ambient magnetic field $\underset{\sim}{B} = B\,\hat{e}_y$).

$$\frac{dV_{px}}{dt} = \frac{eE_x}{m_p} + \Omega_p V_{pz} - \nu^*(V_{px} - V_b) \qquad (1)$$

where the subscript p refers to solar wind protons, $\Omega_p = eB/m_pc$, ν^* is an anomalous ion-ion collision frequency, $\underset{\sim}{V}_b = V_b\,\hat{e}_x$ is the streaming barium velocity, e is the charge, and m is the mass. The first term on the RHS of (1) arises from a laminar electric field usually associated with the leading edge of the magnetic compression; it acts to accelerate barium ions and to slow down solar wind protons. The second term is the magnetic force which is associated with Larmor coupling. The final term corresponds to turbulent "pick up" of the solar wind and arises because of plasma instabilities. For plasma turbulence such that $\nu^* > \Omega_i$ it is clear that turbulent coupling can dominate over Larmor coupling. Also, notice that the force $\Omega_p V_{pz}$ associated with Larmor coupling is proportional to the value of V_{pz} and will be very weak as long as $V_{pz} \approx 0$. The time evolution of V_{pz} is given by

$$\frac{dV_{pz}}{dt} = \frac{eE_z}{m_p} = \frac{eV_{px}B}{m_pc} = \Omega_p V_{px} \qquad (2)$$

In deriving (2) we assume $E_z = V_{px}B/c$ which is the motional electric field of the solar wind.

The subject of the appropriate value of ν^* and the dominant instability that drives it has been extensively studied. We refer the interested reader to Lampe et al. (1975) and summarize only the key conclusions. The counterstreaming between the barium ions and solar wind protons generates a local velocity distribution function such as shown in Fig. 5. Figure 5 is drawn for convenience in the solar wind reference frame. For singly ionized barium the electrons have a relative velocity $\underset{\sim}{V} = V_e\,\hat{e}_x$ with respect to the solar wind protons given by $V_e = V_{px}(n_b/n_e)$ where n_b is the density of the barium and $n_e = n_b + n_p$.

The dispersion equation for this situation is given by (Papadopoulos et al., 1971)

$$D(\omega, k) = \frac{\omega_b^2}{k^2 v_b^2} Z'\left(\frac{\omega - kV_{px} \cos\theta}{kv_b}\right) + \frac{\omega_p^2}{k^2 v_p^2} Z'\left(\frac{\omega}{kv_p}\right)$$

$$+ 1 + \frac{\omega_e^2}{\Omega_e^2}\left[1 + \frac{\omega_e^2}{c^2k^2}(1 + \beta_e)^{-1}\right] = 0 \qquad (3)$$

where $\omega_\alpha = (4\pi n_\alpha e^2/m_\alpha)^{1/2}$ is the plasma frequency and $v_\alpha = (T_\alpha/m_\alpha)^{1/2}$ is the thermal speed of species α (e: electron, b: barium; p: proton), $\underset{\sim}{k} = k_x \hat{e}_x + k_z \hat{e}_z$, $\theta = \tan^{-1}(k_z/k_x)$, $\underset{\sim}{V}_p = V_{px} \hat{e}_x$, $\Omega_e = eB/m_e c$ is the electron cyclotron frequency, $\beta_e = 8\pi n_e T_e/B^2$ and $Z'(\zeta) = -2(1 + \zeta Z(\zeta))$ with Z the plasma dispersion function. In writing (3) we have assumed $\underset{\sim}{k} \cdot \underset{\sim}{B} = 0$ (i.e., $k_y = 0$) so that we are only considering flute modes, and have assumed that the ions are unmagnetized (valid for $\omega > \Omega_{p,b}$ and $k\rho_{p,b} \gg 1$ where $\rho_{p,b}$ is the mean ion Larmor radius of the protons and barium ions, respectively) and the electrons are magnetized. We comment that retaining a finite k_y can generate the modified two stream instability via V_e (McBride et al., 1972). However, this instability produces little momentum coupling between the counterstreaming ions; it primarily heats electrons and generates electron tails parallel to $\underset{\sim}{B}$.

We can simplify (3) by assuming cold ions, i.e., $v_b \ll \omega/k - V_{px}\cos\theta$ and $v_p \ll \omega/k$. In this limit $Z(\zeta) = -1/\zeta - 1/2\zeta^3$ and (3) can be written as

$$\frac{\alpha\omega_{Hp}^2}{(\omega - \underset{\sim}{k}\cdot\underset{\sim}{V}_p)^2} + \frac{\omega_{Hp}^2}{\omega^2} = 1 + \frac{\omega_0^2}{k^2c^2} \qquad (4)$$

where the proton lower hybrid frequency is

$$\omega_{Hp}^2 = \omega_p^2(1 + \omega_e^2/\Omega_e^2)^{-1} \qquad (5a)$$

$$\alpha = \frac{n_b}{n_p}\frac{m_p}{m_b} \qquad (5b)$$

and

$$\omega_0^2 = \frac{\omega_e^2}{\Omega_e^2}\frac{\omega_e^2}{(1 + \omega_e^2/\Omega_e^2)(1 + \beta_e)} \qquad (5c)$$

Notice that as long as $n_b/n_p < m_b/m_p \approx 137$ then $\alpha < 1$ and the small term in the dispersion relation is due to barium ions. This implies that when $n_b/n_p < 137$ the excited waves will be proton, rather than barium, lower hybrid waves.

For $\alpha < 1$ and $\omega_0^2 << c^2k^2$, the most unstable waves have the following approximate frequency and wavenumber

$$\omega_r \approx \omega_{Hp} \tag{6a}$$

$$\gamma \approx 0.69\,\alpha^{1/3}\omega_{Hp} \tag{6b}$$

$$k \cos\theta \approx \omega_{Hp}/V_{px}. \tag{6c}$$

On the other hand, for values of ω_0^2/c^2k^2 sufficiently large, the modes can be stabilized because of electromagnetic effects (Papadopoulos et al., 1971; Lampe et al., 1975). The criterion for instability is given by

$$\cos\theta < \frac{c\omega_{Hp}}{V_{px}\omega_e}\left(1 + \alpha^{1/3}\right)^{3/2}\left(1 + \beta_e\right)^{1/2} \equiv \cos\theta_0. \tag{7}$$

For the parameters of interest, we note that $\alpha << 1$ and $\beta_e << 1$ and (7) can be rewritten as

$$\cos\theta < \frac{V_{Ap}}{V_{px}}\left(1 + \frac{n_b}{n_p}\right)^{-1} \tag{8}$$

where $V_{Ap} = B/(4\pi n_p m_p)^{1/2}$ is the local Alfvén velocity associated with the protons. Notice that the angle θ_0 separates the angular region of unstable modes from stable modes in the plane perpendicular to the magnetic field (Fig. 6). For values of the RHS of (8) which are comparable to or larger than unity, the entire k-space plane is unstable, and as shown in Lampe et al. (1975), complete ion-ion momentum coupling accompanies the interaction. The instability weakens substantially when the stable region around $\underset{\sim}{V}_p$ increases (i.e., θ_0 increases) leaving only weak off angle modes unstable.

To better illustrate the linear properties of the counterstreaming ion-ion instability, we present numerical solutions of (3) for parameters relevant to the AMPTE release of Dec. 27, 1984. In Figs. 7 and 8 we take

$m_b/m_p = 137$, $v_p/V_{px} = 0.3$, $v_b/V_{px} = 0.01$, and $\beta_e = 0.0$. The most significant variations are for n_b/n_p and V_{Ap}/V_{px} so we present results for a range of values for these parameters. In Figs. 7 and 8 we plot γ_M/ω_{Hp} vs V_{Ap}/V_{px} for $n_b/n_p = 0.5$, 2.0, 5.0 and 10.0 (or $\alpha = 3.7 \times 10^{-3}$, 1.5×10^{-2}, 3.7×10^{-2}, and 7.4×10^{-2}, respectively). In Fig. 7 we consider $\theta = 0°$, while in Fig. 8 we consider $\theta = 60°$. Here γ_M is the maximum growth rate as a function of k. We have not plotted ω_r or k but note that (6a) and (6c) are in reasonable agreement with the numerical values. In Fig. 7 we note the following. First, in the limit $V_{Ap}/V_{px} \gg 1$, the growth rate asymptotes to its maximum value which is approximately given by (6b) [e.g., for $n_b/n_p = 0.5$ ($\alpha = 3.7 \times 10^{-3}$) we obtain $\gamma_M/\omega_{Hp} = 0.108$]. Also, in this limit we note that the maximum growth rate increases as n_b/n_p increases. Second, as V_{Ap}/V_{px} decreases the growth rate decreases; for sufficiently small values of V_{Ap}/V_{px} the modes are stabilized because of electromagnetic effects. However, note that the critical value of V_{Ap}/V_{px} which stabilizes the modes decreases with decreasing n_b/n_p (e.g., for $V_{Ap}/V_{px} = 2$ the mode is stable for $n_b/n_p = 10.0$ but unstable for $n_b/n_p = 0.5$). This is consistent with (8) which, for $\theta = 0$, can be written as $V_{Ap}/V_{px} > (1 + n_b/n_p)$. We also note that the critical value of V_{Ap}/V_{px} predicted by (8) is somewhat greater than is found from Fig. 7. That is, for $n_b/n_p = 0.5$, 2.0, 5.0, and 10.0, (8) predicts $\gamma = 0$ for $V_{Ap}/V_{px} = 1.5$, 3.0, 6.0, and 11.0, respectively; however, Fig. 7 shows that $\gamma = 0.01\ \omega_{HP}$ (≈ 0) for $V_{Ap}/V_{px} =$ 1.2, 2.0, 3.6, and 5.5. The reason for this is that (8) is based upon the assumption of co' protons $(\omega \gg kv_p)$ but for the parameters used in Fig. 7 (i.e., $v_p/V_{px} = 0.3$) this assumption breaks down as V_{Ap}/V_{px} decreases and thermal effects allow the modes to grow in the stable "cold" plasma regime.

In Fig. 8 we plot γ_M/ω_{Hp} vs. V_{Ap}/V_{px} for the same parameters as in Fig. 7 but we consider $\theta = 60°$. The basic features of Fig. 8 are the same as Fig. 7. However, two points are worth mentioning. First, and most important, unstable modes exist for values of V_{Ap}/V_{px} that lead to stable modes in the case of $\theta = 0$. In fact, for all values of n_b/n_p considered, strong growth (i.e., $\gamma > 0.01\ \omega_{Hp}$) exists for $V_{Ap}/V_{px} > 2$, and in the case of $n_b/n_p = 0.5$ exists for $V_{Ap}/V_{px} > 0.5$. Again, this behavior is consistent with (8). Second, we note that for the same values of n_b/n_p, the maximum growth rates are smaller for $\theta = 60°$ than $\theta = 0°$. This appears to be inconsistent with (6b) which indicates the maximum growth rate does

not depend upon angle. The reason for the discrepancy is the effect of thermal protons which have a stabilizing influence because of ion Landau damping. Finally, we note that we have chosen $\theta = 60°$ because nonlinear studies have demonstrated that if the angular region of unstable waves initially satisfied the condition $\cos\theta < \cos\theta_0 = 0.5$ (i.e., $\theta_0 = 60°$) then the entire k-plane subsequently becomes unstable resulting in complete momentum coupling between the ion streams. If $\cos\theta > 0.5$ then the situation, although mildly unstable, is quickly stabilized by finite temperature effects with little momentum coupling.

IV. COMPARISON BETWEEN THEORY AND OBSERVATIONS

We now proceed to analyze the observations with the theoretical models described in Section III. Our approach is to examine in detail the key times marked as 1-4 in Figs. 2 and 3. Table 1 gives the values of the important plasma parameters. We note that all of the data are not well known and we have made estimates of some values. Also, in comparing the theoretical conditions for instability with experimentally observed parameters, one does not expect to find "grossly" unstable conditions since the turbulence observed is generally in the nonlinear regime (i.e., near marginal stability).

The slowing down of the solar wind begins at the point marked 1 in Figs. 2 and 3. From Table 1 we see that $n_b/n_p = 0.2$ and $V_{Ap}/U_p = 0.4$; from Fig. 8 note that these conditions are marginally stable for the ion-ion instability. Therefore the beginning of the interaction is consistent with the minimum condition for a momentum coupling cross field, counterstreaming proton-barium instability. The theoretically expected electrostatic waves cover the range between $f_{Hp} \approx 10$ Hz and $f_{ce} \approx 560$ Hz, with most of the energy confined in the 15-40 Hz region. At the time marked 2 (UT 12:35:15) the magnetic field compression starts and there is an attendant increase in V_{Ap}/V_{px}. Thus, this leads to conditions more favorable to instability and we expect the entire k-plane to become unstable leading to strong momentum coupling. Figures 2 and 3 seem to confirm this. The range of the unstable waves corresponds to 22 Hz - 1.6 kHz with the most of the energy in the 22 - 60 Hz region. Notice that between times marked 1 - 3, the value of V_{pz} is relatively unchanged and remains close to zero, while V_{px} is reduced

sharply. The ion-ion driven interaction seems to terminate at the time marked 3 (UT 12:34:27). At this time the solar wind speed is $|V_{px}| \approx 250$ km/sec; the protons have lost more than 80% of their initial energy. We comment that the proton temperature is of the order 5×10^6 °K so that the proton thermal speed is $v_p \approx 200$ km/sec and the wave modes are subsequently suppressed because of proton Landau damping. This is consistent with the wave measurements shown in Fig. 4. Following the time marked 3 (UT 12:34:27) till 4 (UT 12:33:50) the value of V_{px} continues to decrease to almost zero. However, the data are indicative of a different interaction. The slowing down is characterized by very weak electrostatic activity and most important, by an increase in the value of V_{pz} which reaches 250 km/sec when V_{px} approaches zero. This is the type of interaction expected from Larmor coupling described by (1) and (2) for $\nu^* < \Omega_p$. It is basically a gyration of the protons about the magnetic field which is piled up in the front of the barium cloud. This stage is followed by entry into the magnetic cavity. We can associate the observed sunward flux of 0.5 keV protons with the thermal expansion of the protons when V_{px} became small.

The detailed spectrum presented in Fig. 4 allows a further comparison with theoretical concepts. As noted before, the instability saturates by trapping. For the proton-barium situation and with $\alpha \ll 1$ the phase velocity V_{ph} of the unstable waves lies near the barium flow velocity (see Fig. 6). In the solar wind reference frame we note that (Lampe et al., 1975)

$$V_{ph} = V_{px}\left(1 - 2^{-4/3}\, \alpha^{1/3}\right) \tag{9}$$

Waves growing with this phase velocity will trap protons when their potential is of the order of

$$e\Phi \approx \frac{1}{2}\, m_p V_{ph}^2 \approx \frac{1}{2}\, m_p V_{px}^2 \tag{10a}$$

and barium when

$$e\Phi \approx \frac{1}{2}\, m_b \left(\frac{\alpha}{2}\right)^{2/3} V_{px}^2 . \tag{10b}$$

By comparing (10a) and (10b) we find that as long as

$$\frac{n_b}{n_p} > 2\left(\frac{m_p}{m_b}\right)^{1/2} \approx 0.17 \qquad (11)$$

the condition for proton trapping (10a) will be reached first and will saturate the instability. Since in our case (11) is satisfied, we expect that the instability will saturate by trapping the protons. This is similar to the saturation of the Buneman instability studied by Davidson et al. (1970) which saturates by trapping electrons rather than protons, despite the fact that V_{ph} is near the proton beam. The amplitude of the electric field required to trap the protons is

$$\tilde{E} \approx \frac{1}{4} \frac{m_p V_{px}}{e} \omega_{Hp}. \qquad (12)$$

For the parameters given in Table I (i.e., V_{px} = 250 - 400 km/sec and ω_{Hp} = 107 - 145 sec^{-1}) we find that (12) predicts $\tilde{E} \approx$ 67 - 145 mV/m. Gurnett et al. (1985) report values of $\tilde{E} \approx$ 140 mV/m while noting that the 10 Hz channel was saturated. Thus, these field values are consistent with the saturation by trapping. Note that the peak spectral density in Fig. 5 is $\lesssim$ 20 Hz which is consistent with theoretical values. The value of ν^* can be estimated on the basis of the wave spectral energy density $S(\omega)$ in the lower hybrid region, as given in Fig. 4. It is approximately given by (Papadopoulos, 1977)

$$\nu^* \approx \frac{D}{(V_{px} - V_{ph})^2} \approx \frac{e^2}{m_p^2} \frac{S(\omega \approx \omega_{Hp})}{V_{px}^2} \approx$$

$$\approx 100 \left(\frac{100\ \text{km/sec}}{V_{px}}\right)^2 \left(\frac{S(\omega \approx \omega_{Hp})}{10^{-4}\ V^2/m^2 Hz}\right)$$

where D is the diffusion coefficient in velocity space. For the measured values at 12:34:27 and $S(\omega \approx \omega_{Hp})$ given by Fig. 4 we find $\nu^* \approx$ 12 - 20 so that $\nu^* \gg \Omega_p, \Omega_b$.

V. SUMMARY AND CONCLUSIONS

We have presented an analysis of previously reported observations on the solar wind-barium interaction associated with the AMPTE artificial comet release of Dec. 27, 1984. Based on these results we have argued that

the solar wind couples momentum (and energy) to the barium ions through both laminar and turbulent processes [see (1)]. The laminar forces acting on the particles are the laminar electric and magnetic fields; the turbulent forces are associated with the intense electrostatic wave activity. This wave activity has been shown to be caused by a cross-field proton-barium ion streaming instability. The observed wave frequencies and saturated amplitudes are consistent with our theoretical analysis.

The following picture emerges. After the barium is released from the canisters, it expands outward and is photoionized. The expanding barium cloud forms a compressed density and magnetic field region on the sunward side of the expansion. As the solar wind protons stream into this region they first interact with the barium ions to generate relatively weak off-angle electrostatic turbulence. This occurs when $n_b/n_p \lesssim 1$ and $V_{ap}/V_{px} \lesssim 1$. This turbulence acts to couple the solar wind protons and barium ions, and the protons slow down (see in Fig. 1 between marks 1 and 2). As the protons move deeper into barium ion shells they encounter the compressed magnetic field region (which increases the local proton Alfvén speed) and a more dense barium ion region (which increases n_b/n_p). These two factors allow stronger wave growth to occur; this corresponds to the intense wave activity observed between the times marked 2 and 3 on Fig. 3. This turbulence causes the solar wind protons to slow down even more, and also produces proton and barium ion heating. Finally, the protons undergo a gyration about the compressed magnetic field which is indicated by a decrease in V_{px} and an increase in V_{pz}. We expect a similar type of interaction to occur in the solar wind-comet interaction. This topic is currently under study and will be reported elsewhere.

There are two more points that we would like to address. The first is about the electron heating and electron acceleration. The observed electron heating seems consistent with adiabatic heating. However, in addition to the local heating, the UK spacecraft observed electron fluxes with energy larger than 100 eV, i.e., the period between our marks 1-3. This is the period during which the lower hybrid instability was operating. For the flute mode ($k_y = 0$) instability discussed above, the electrons are adiabatic. However, field aligned suprathermal electron tails can be produced by the non-flute modes ($k_y \neq 0$), corresponding to the

electron-ion modes mentioned in Section III. These modes have frequencies typically 5-6 f_{Hp} and saturate at a lower level. The details of this interaction will be discussed elsewhere. It is sufficient here to note that the existence of wave frequencies in the 200 Hz to 1 kHz range is consistent with the model and with the electron fluxes observed by the UK spacecraft. Second, although the solar wind barium interaction results in complete momentum coupling, the barium has not been picked up by the solar wind during the 3-4 min of the measurements. This is due to the large barium mass and density which would require times of the order of 8-10 min to be picked up. This should be contrasted with the lithium releases for which pick up occured at much shorter times.

The AMPTE data presented supports both the laminar and turbulent coupling mechanisms that have been proposed for debris-air coupling following a HANE (Longmire, 1963; Lampe et al., 1975; Goodrich et al., 1985). To our knowledge, this is the only experimental data which unambiguously demonstrates the various coupling mechanisms, and lends strong support to the HANE coupling models developed at NRL. Furthermore, it is indicative of the type of data that would be valuable in understanding the DNA/NRL early time experiment; well resolved data on the evolution of the magnetic field, particles, and wave activity. Finally, the good agreement between theory and data suggests that other data involving the coupling of counterstreaming plasmas be examined; specifically, the recent data obtained from the space missions to Halley's comet should be investigated with regard to the physics of HANEs.

Acknowledgment

We appreciate valuable discussions on the AMPTE observations with Drs. G. Haerendel, G. Paschmann, S.M. Krimigis, and D.A. Gurnett. This research has been supported by NASA (K.P. and A.T.Y.L.), and ONR and DNA (J.D.H.).

REFERENCES

Davidson, R.C., N.A. Krall, K. Papadopoulos, and R. Shanny, "Electron heating by electron-ion beam instabilities," Phys. Rev. Lett., 24, 579, 1970.

Fedder, J.A., J.G. Lyon, and J.L. Giuliani, Jr., "Numerical simulations of comets: Predictions for comet Giacobini-Zinner," EOS, 67, 17, 1986.

Goodrich, C., K. Papadopoulos, and J.D. Huba, "Early time coupling studies using a 1D hybrid code," NRL Memo Rept. 5553, 1985.

Gurnett, D.A., R.R. Anderson, B. Häusler, G. Haerendel, O.H. Bauer, R.A. Treumann, H.C. Koons, R.H. Holzworth, and H. Lühr, "Plasma waves associated with the AMPTE artificial comet," Geophys. Res. Lett., 12, 851, 1985.

Haerendel, G., G. Paschmann, W. Baumjohann, and C.W. Carlson, "Dynamics of the AMPTE artificial comet," Nature, 320, 720, 1986.

Ip, W.-H. and W.I. Axford, "Theories of physical processes in the cometary comae and ion tails," in Comets, edited by L.L. Wilkening, University of Arizona Press, Tucson, 1982.

Lampe, M., W.M. Manheimer, and K. Papadopoulos, "Anomalous transport coefficients for HANE applications due to plasma microinstabilities," NRL Memo. Rept. 3076, 1975.

Longmire, C.L., "Notes on debris-air-magnetic interaction," The RAND Corporation Report RM-3386-PR, 1963. AD296597.

Mendis, D.A. and H.L.F. Houpis, "The cometary atmosphere and its interaction with the solar wind," Rev. Geophys., 20, 885, 1982.

McBride, J.B., E. Ott, J.P. Boris, and J.H. Orens, "Theory and simulation of turbulent heating by the modified two-stream instability," Phys. Fluids, 15, 2367, 1972.

Papadopoulos, K., Review of anomalous resistivity for the ionosphere, Rev. of Geophys. and Space Phys., 15, 113, 1977.

Papadopoulos, K., R. Davidson, J.M. Dawson, I. Haber, D.A. Hammer, N.A. Krall, and R. Shanny, "Heating of counterstreaming ion beams in an external magnetic field," Phys. Fluids, 14, 849, 1971.

Sagdeev, R.Z., V.D. Shapiro, and V.I. Shevchenko, "MHD turbulence in the solar wind-comet interaction region," Geophys. Res. Lett., 13, 85, 1986.

Valenzuela, A., G. Haerendel, H. Föppl, F. Melzner, H. Neuss, E. Rieger, J. Stöcker, O. Bauer, H. Höfner, and J. Loidl, "The AMPTE artificial comet experiments," Nature, 320, 700, 1986.

TABLE I

Plasma Parameters for the 27 Dec. 1984 AMPTE Release

UT	V_{px} (km/sec)	V_{pz} (km/sec)	B (γ)	n_e (cm^{-3})	n_p (cm^{-3})	n_{Ba} (cm^{-3})	f_{Hp} (hz)	V_{Ap} (km/sec)
12:36:20	-550	0	20	6*	5	1*	12	195
12:35:15	-400	0	50	20*	10*	10*	23	345*
12:34:27	-250	- 50	85	110	10*	100	17	586*
12:33:50	- 75	-250	130	3010	10*	3000	5	896*

*Estimate

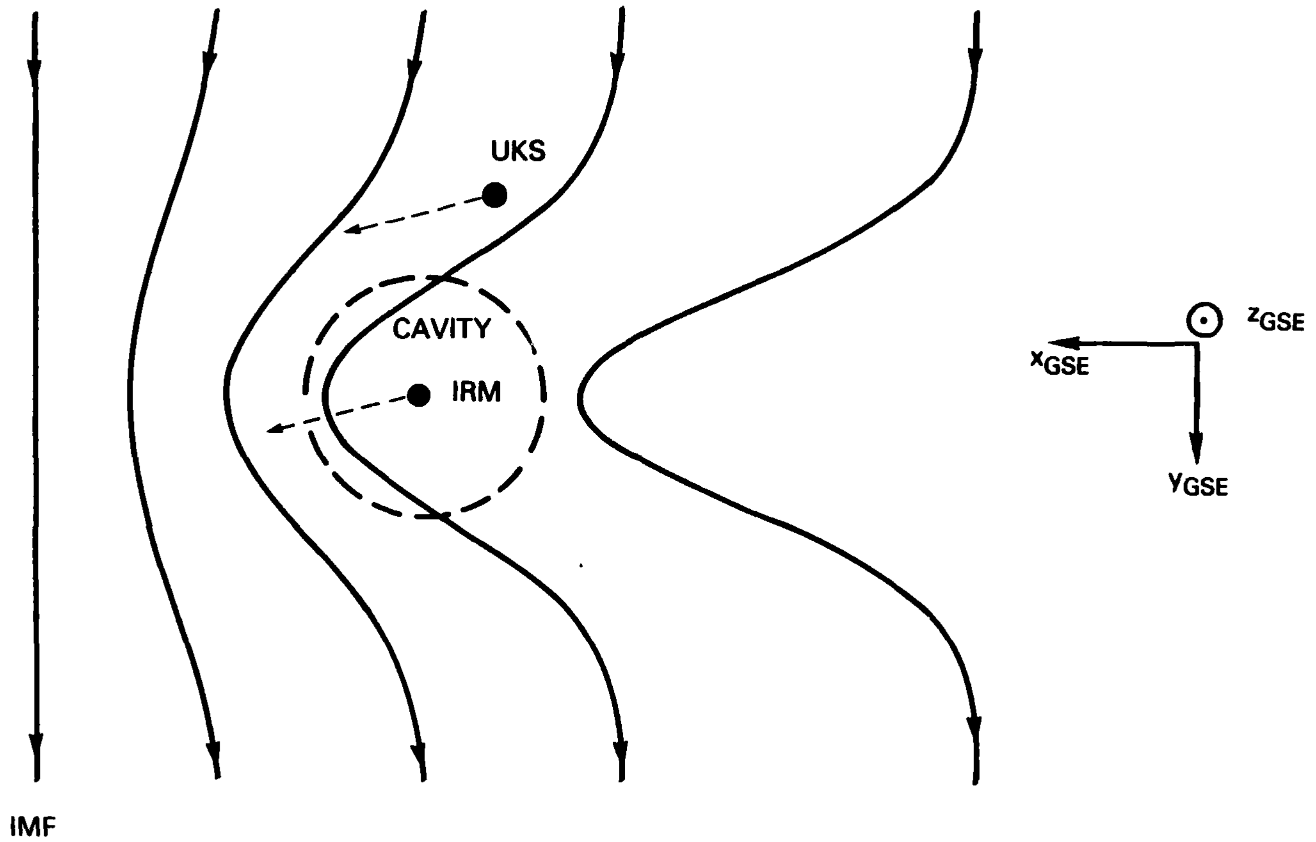

Fig. 1 – Schematic of the spacecraft positions and magnetic field structure for the Dec. 27, 1984 AMPTE release.

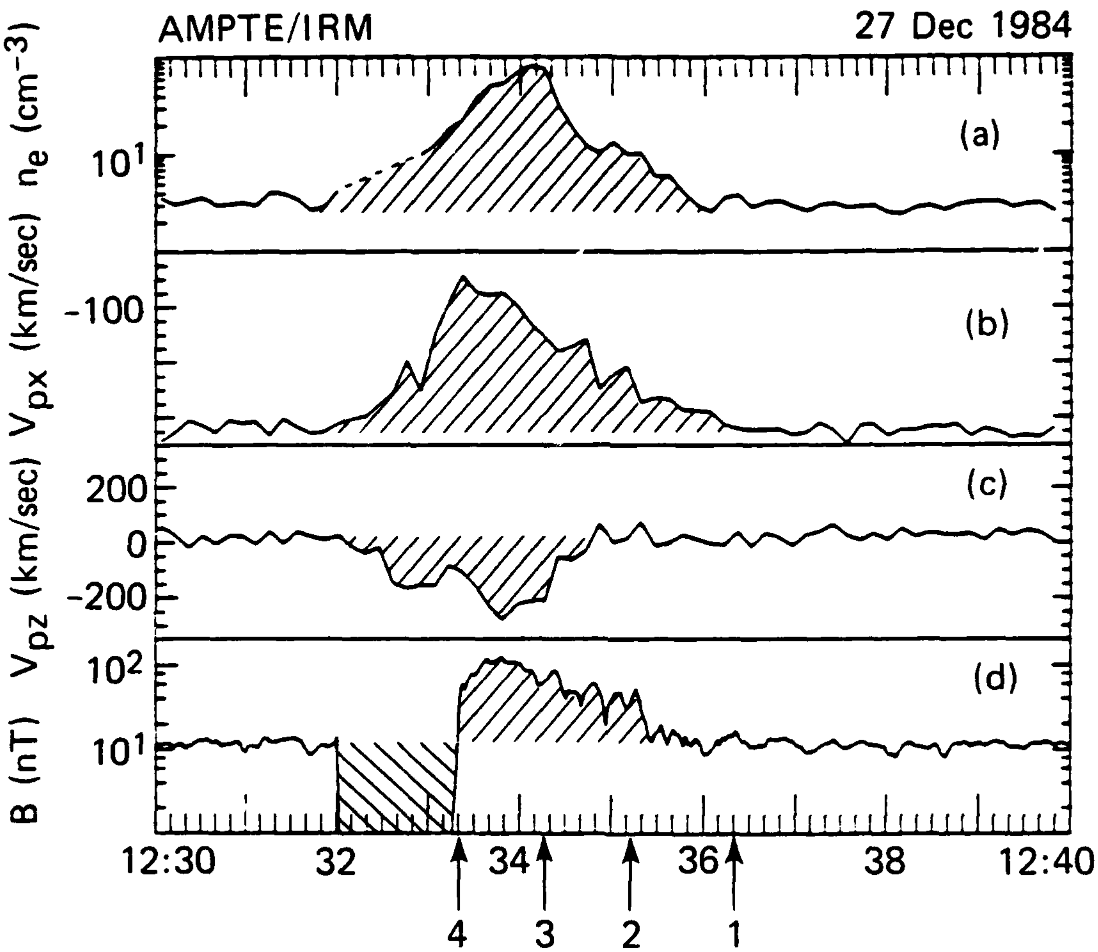

Fig. 2 – Particle and field data (from Haerendel et al., 1986).

(a) Electron density (cm^{-3}). (b) Solar wind proton velocity (km/sec) in the x-direction (GSE coordinates). (c) Solar wind proton velocity (km/sec) in the y-direction (GSE coordinates). (d) Magnetic field (nT).

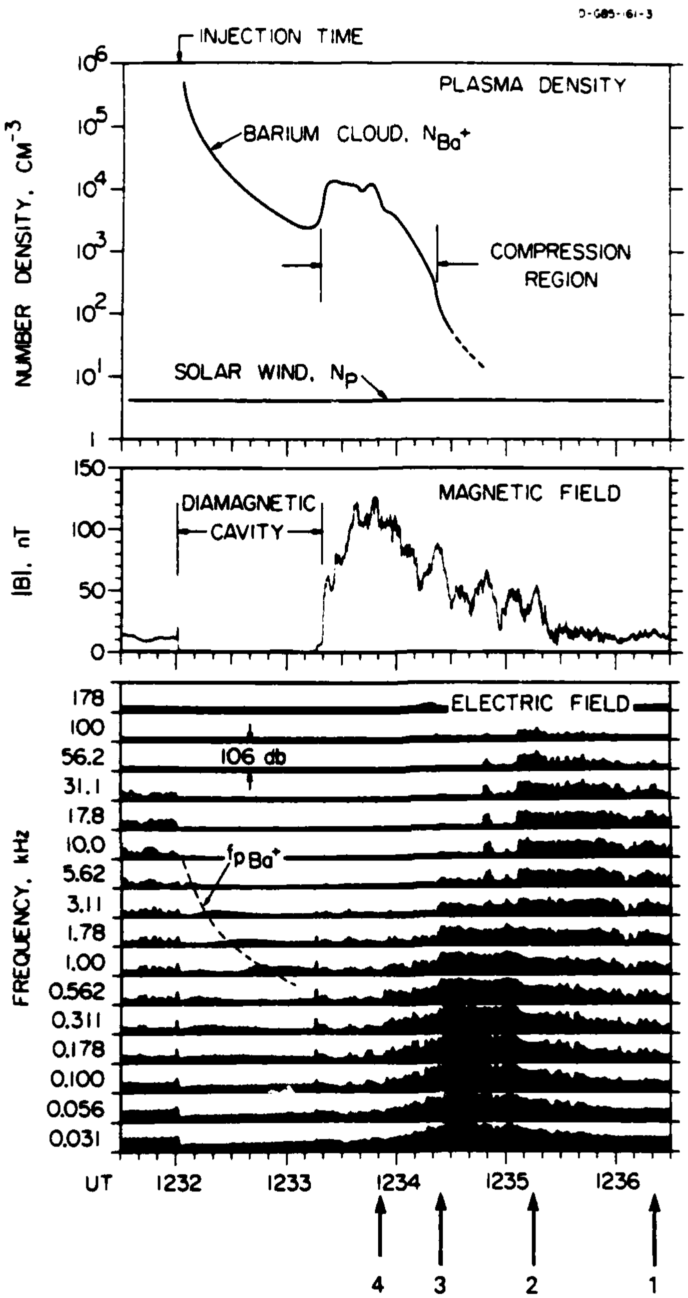

Fig. 3 — Particle, field, and electric field wave data (from Gurnett et al., 1985). The barium ion density is based upon emissions at the plasma frequency. Note the intense, low frequency (f ~ 30 Hz - 1 kHz) electrostatic waves during between the times marked 2 and 3.

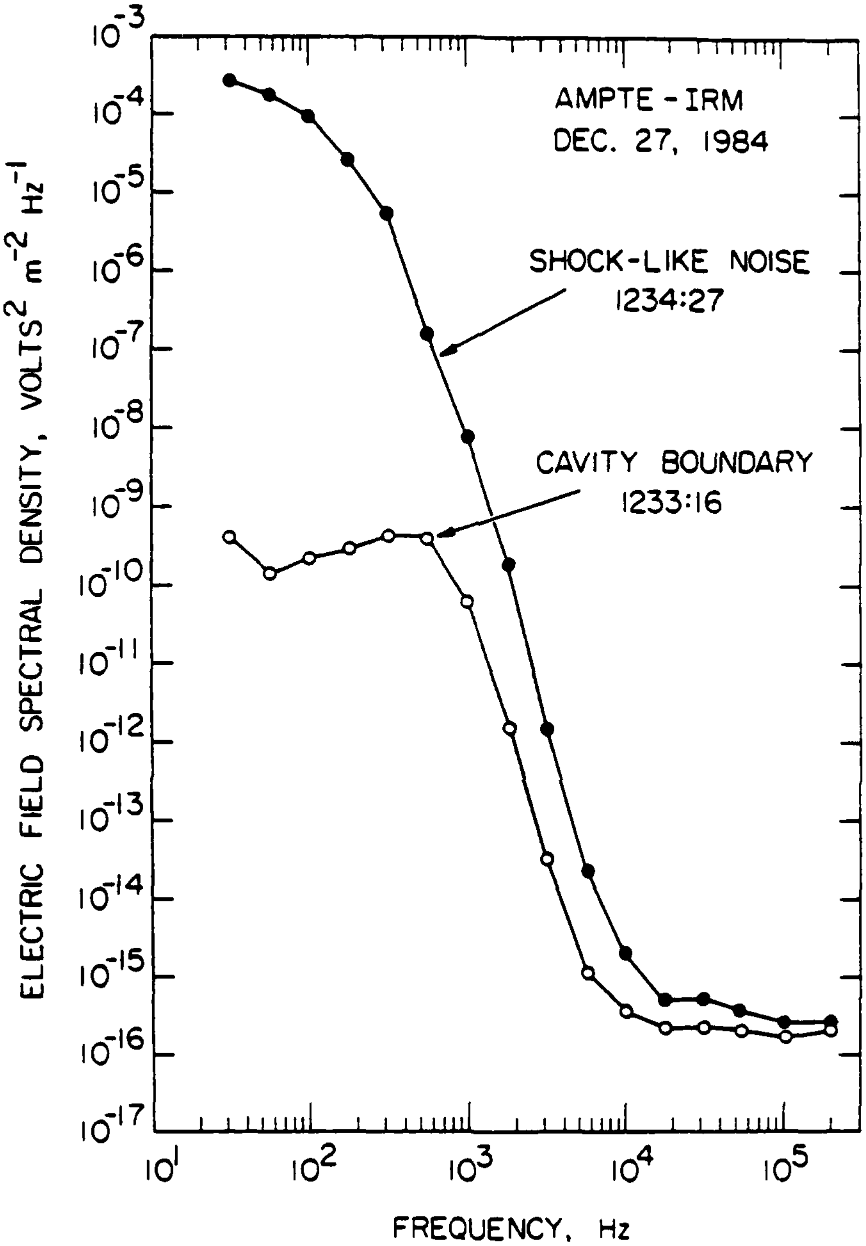

Fig. 4 — Electric field spectral density as a function of frequency for times UT 12:34:27 and UT 12:33:16 (from Gurnett et al., 1985). Note that the most intense waves for UT 12:34:27 (marked 3 on Figs. 2 and 3) are low frequency (i.e., f ~ 30 Hz).

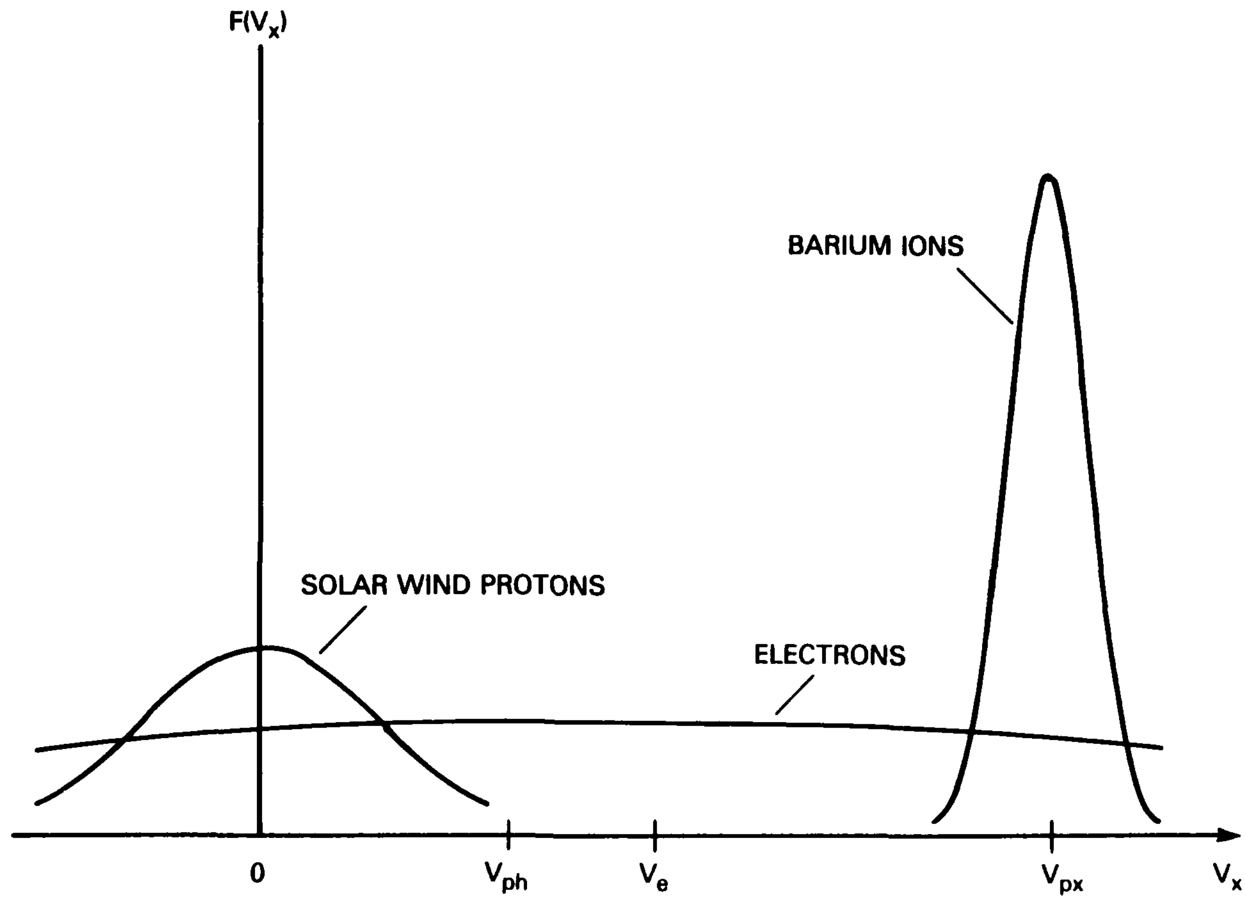

Fig. 5 — Local velocity distributions of the solar wind protons, barium ions, and electrons in the solar wind frame of reference.

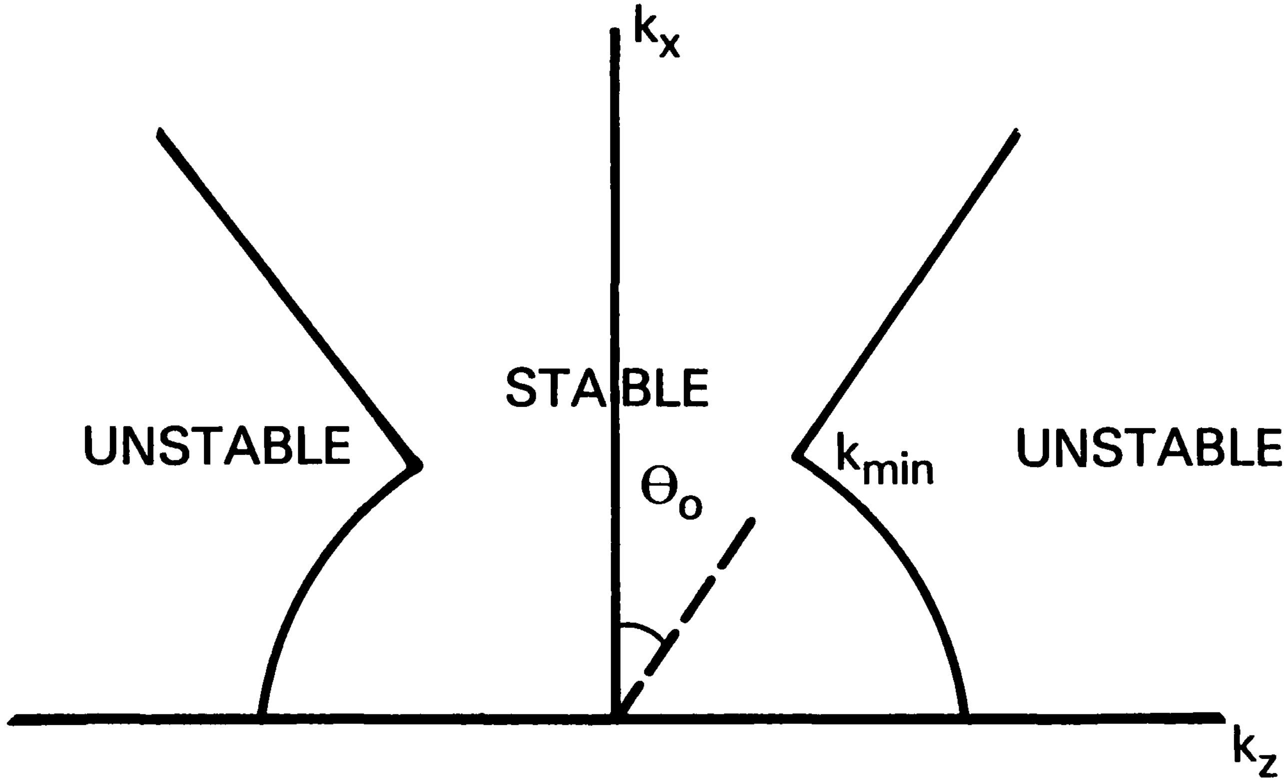

Fig. 6 — Schematic of unstable waves driven by the magnetized ion-ion instability in the k_x - k_z plane. The relative drift between ions is in the x-direction.

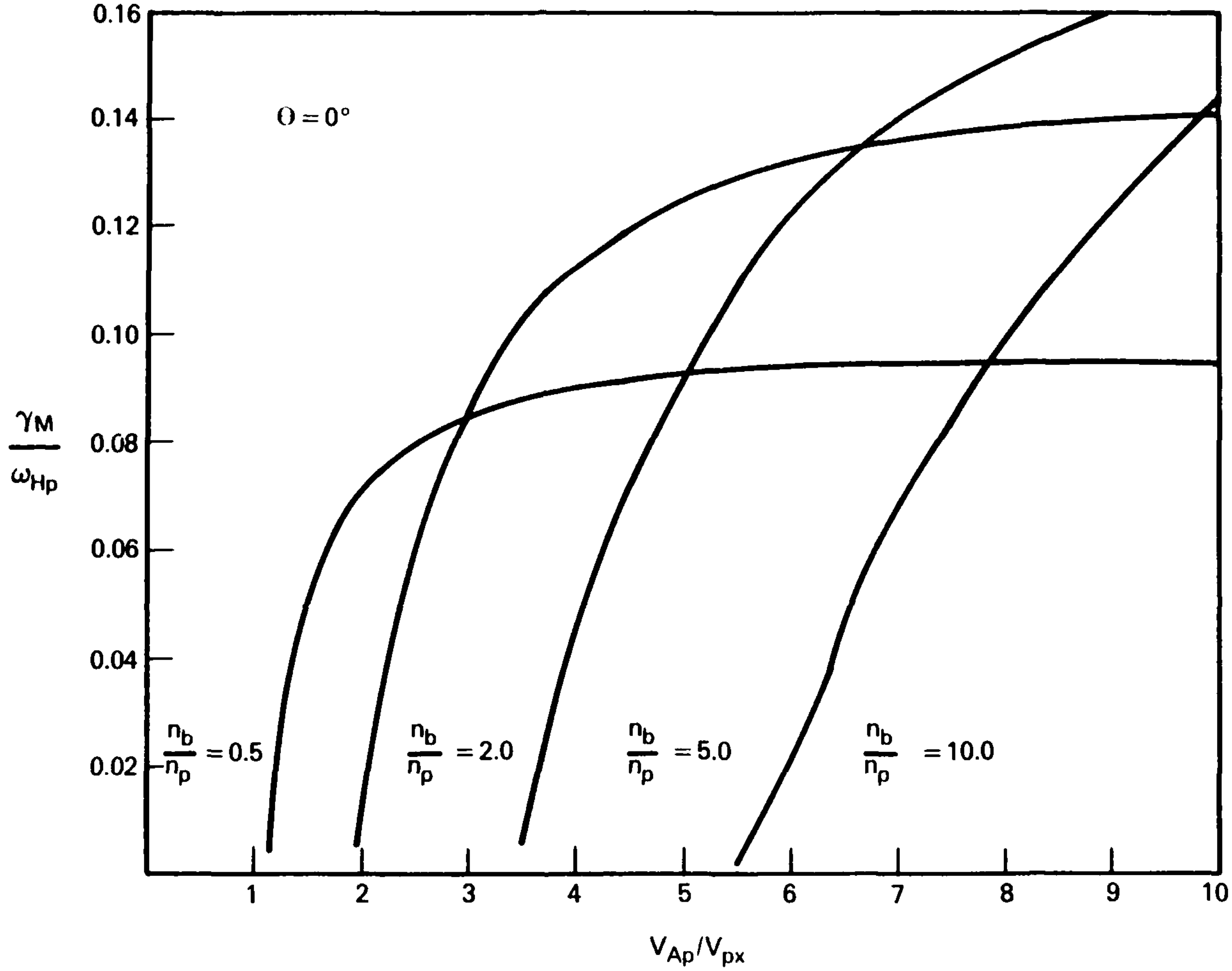

Fig. 7 — Plot of γ_M/ω_{Hp} vs V_{ap}/V_{px} for $\theta = 0°$ and $n_b/n_p = 0.5, 2.0, 5.0, 10.0$. Here γ_m is the maximum growth rate with respect to the wavenumber k.

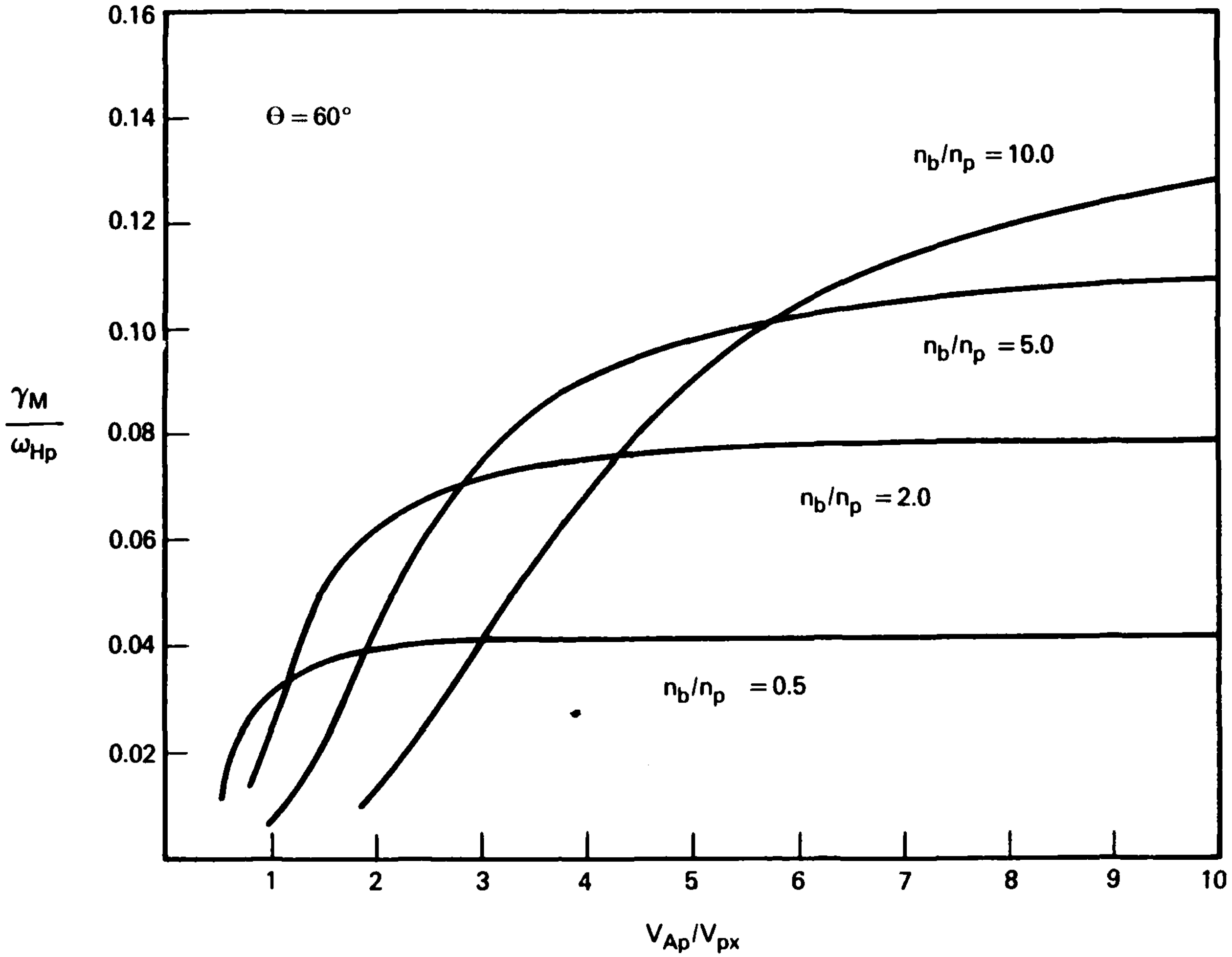

Fig. 8 — Plot of γ_M/ω_{Hp} vs. V_{Ap}/V_{px} for $\theta = 60°$ and $n_b/n_p = 0.5, 2.0, 5.0, 10.0$. Note that for these parameters ($\theta = 60°$), the modes are excited for lower values of V_{Ap}/V_{px} than in the previous case ($\theta = 0°$), consistent with (8).

DISTRIBUTION LIST

DEPARTMENT OF DEFENSE

ASSISTANT SECRETARY OF DEFENSE
COMM, CMD, CONT 7 INTELL
WASHINGTON, DC 20301

DIRECTOR
COMMAND CONTROL TECHNICAL CENTER
PENTAGON RM BE 685
WASHINGTON, DC 20301
  01CY ATTN C-650
  01CY ATTN C-312 R. MASON

DIRECTOR
DEFENSE ADVANCED RSCH PROJ AGENCY
ARCHITECT BUILDING
1400 WILSON BLVD.
ARLINGTON, VA 22209
  01CY ATTN NUCLEAR
    MONITORING RESEARCH
  01CY ATTN STRATEGIC TECH OFFICE

DEFENSE COMMUNICATION ENGINEER CENTER
1860 WIEHLE AVENUE
RESTON, VA 22090
  01CY ATTN CODE R410
  01CY ATTN CODE R812

DIRECTOR
DEFENSE NUCLEAR AGENCY
WASHINGTON, DC 20305
  01CY ATTN STVL
  04CY ATTN TITL
  01CY ATTN DDST
  03CY ATTN RAAE

COMMANDER
FIELD COMMAND,
DEFENSE NUCLEAR AGENCY
KIRTLAND, AFB, NM 87115
  01CY ATTN FCPR

DEFENSE NUCLEAR AGENCY
SAO/DNA
BUILDING 20676
KIRTLAND AFB, NM 87115
  01CY D.C. THORNBURG

DIRECTOR
BMD ADVANCED TECH CTR
HUNTSVILLE OFFICE
P.O. BOX 1500
HUNTSVILLE, AL 35807
  01CY ATTN ATC-T MELVIN T. CAPPS
  01CY ATTN ATC-O W. DAVIES
  01CY ATTN ATC-R DON RUSS

DIRECTOR
INTERSERVICE NUCLEAR WEAPONS SCHOOL
KIRTLAND AFB, NM 87115
  01CY ATTN DOCUMENT CONTROL

JOINT PROGRAM MANAGEMENT OFFICE
WASHINGTON, DC 20330
  01CY ATTN J-3 WWMCCS EVALUATION
    OFFICE

DIRECTOR
JOINT STRAT TGT PLANNING STAFF
OFFUTT AFB
OMAHA, NB 68113
  01CY ATTN JSTPS/JLKS
  01CY ATTN JPST G. GOETZ

CHIEF
LIVERMORE DIVISION FLD COMMAND DNA
DEPARTMENT OF DEFENSE
LAWRENCE LIVERMORE LABORATORY
P.O. BOX 808
LIVERMORE, CA 94550
  01CY ATTN FCPRL

COMMANDANT
NATO SCHOOL (SHAPE)
APO NEW YORK 09172
  01CY ATTN U.S. DOCUMENTS OFFICER

UNDER SECY OF DEF FOR RSCH & ENGRG
DEPARTMENT OF DEFENSE
WASHINGTON, DC 20301
  01CY ATTN STRATEGIC & SPACE
    SYSTEMS (OS)

COMMANDER/DIRECTOR
ATMOSPHERIC SCIENCES LABORATORY
U.S. ARMY ELECTRONICS COMMAND
WHITE SANDS MISSILE RANGE, NM 88002
  01CY ATTN DELAS-EO, F. NILES

DIRECTOR
U.S. ARMY BALLISTIC RESEARCH
LABORATORY
ABERDEEN PROVING GROUND, MD 21005
  01CY ATTN TECH LIBRARY,
    EDWARD BAICY

COMMANDER
U.S. ARMY SATCOM AGENCY
FT. MONMOUTH, NJ 07703
  01CY ATTN DOCUMENT CONTROL

PROGRAM MANAGER
BMD PROGRAM OFFICE
5001 EISENHOWER AVENUE
ALEXANDRIA, VA 22333
  01CY ATTN DACS-BMT J. SHEA

CHIEF C-E- SERVICES DIVISION
U.S. ARMY COMMUNICATIONS CMD
PENTAGON RM 1B269
WASHINGTON, DC 20310
  01CY ATTN C- E-SERVICES DIVISION

COMMANDER
FRADCOM TECHNICAL SUPPORT ACTIVITY
DEPARTMENT OF THE ARMY
FORT MONMOUTH, N.J. 07703
  01CY ATTN DRSEL-NL-RD H. BENNET
  01CY ATTN DRSEL-PL-ENV H. BOMKE
  01CY ATTN J.E. QUIGLEY

COMMANDER
U.S. ARMY COMM-ELEC ENGRG INSTAL AGY
FT. HUACHUCA, AZ 85613
  01CY ATTN CCC-EMEO GEORGE LANE

COMMANDER
U.S. ARMY FOREIGN SCIENCE & TECH CTR
220 7TH STREET, NE
CHARLOTTESVILLE, VA 22901
  01CY ATTN DRXST-SD

COMMANDER
U.S. ARMY MATERIAL DEV & READINESS CMD
5001 EISENHOWER AVENUE
ALEXANDRIA, VA 22333
  01CY ATTN DRCLDC J.A. BENDER

COMMANDER
U.S. ARMY NUCLEAR AND CHEMICAL AGENCY
7500 BACKLICK ROAD
BLDG 2073
SPRINGFIELD, VA 22150
  01CY ATTN LIBRARY

NAVAL RESEARCH LABORATORY
WASHINGTON, DC 20375
  01CY ATTN CODE 4700 S.L. Ossakow,
    26 CYS IF UNCLASS
    (01CY IF CLASS)
    ATTN CODE 4780 J.D. HUBA, 50
    CYS IF UNCLASS, 01CY IF CLASS
  01CY ATTN CODE 4701 I. VITKOVITSKY
  01CY ATTN CODE 7500
  01CY ATTN CODE 7550
  01CY ATTN CODE 7580
  01CY ATTN CODE 7551
  01CY ATTN CODE 7555
  01CY ATTN CODE 4730 E. MCLEAN
  01CY ATTN CODE 4752
  01CY ATTN CODE 4730 B. RIPIN
  20CY ATTN CODE 2628

COMMANDER
NAVAL SPACE SURVEILLANCE SYSTEM
DAHLGREN, VA 22448
  01CY ATTN CAPT J.H. BURTON

OFFICER-IN-CHARGE
NAVAL SURFACE WEAPONS CENTER
WHITE OAK, SILVER SPRING, MD 20910
  01CY ATTN CODE F31

COMMANDER
U.S. ARMY MISSILE INTELLIGENCE AGENCY
REDSTONE ARSENAL, AL 35809
  01CY ATTN JIM GAMBLE

DIRECTOR
U.S. ARMY TRADOC SYSTEMS ANALYSIS
ACTIVITY
WHITE SANDS MISSILE RANGE, NM 88002
  01CY ATTN ATAA-SA
  01CY ATTN TCC/F. PAYAN JR.
  01CY ATTN ATTA-TAC LTC J. HESSE

COMMANDER
NAVAL ELECTRONIC SYSTEMS COMMAND
WASHINGTON, DC 20360
  01CY ATTN NAVALEX 034 T. HUGHES
  01CY ATTN PME 117
  01CY ATTN PME 117-T
  01CY ATTN CODE 5011

COMMANDING OFFICER
NAVAL INTELLIGENCE SUPPORT CTR
4301 SUITLAND ROAD, BLDG. 5
WASHINGTON, DC 20390
  01CY ATTN MR. DUBBIN STIC 12
  01CY ATTN NISC-50
  01CY ATTN CODE 5404 J. GALET

COMMANDER
NAVAL OCCEAN SYSTEMS CENTER
SAN DIEGO, CA 92152
  01CY ATTN J. FERGUSON

COMMANDER
AEROSPACE DEFENSE COMMAND/DC
DEPARTMENT OF THE AIR FORCE
ENT AFB, CO 80912
  01CY ATTN DC MR. LONG

COMMANDER
AEROSPACE DEFENSE COMMAND/XPD
DEPARTMENT OF THE AIR FORCE
ENT AFB, CO 80912
  01CY ATTN XPDQQ
  01CY ATTN XP

AIR FORCE GEOPHYSICS LABORATORY
HANSCOM AFB, MA 01731
  01CY ATTN OPR HAROLD GARDNER
  01CY ATTN LKB
    KENNETH S.W. CHAMPION
  01CY ATTN OPR ALVA T. STAIR
  01CY ATTN PHD JURGEN BUCHAU
  01CY ATTN PHD JOHN P. MULLEN

AF WEAPONS LABORATORY
KIRTLAND AFT, NM 87117
  01CY ATTN SUL
  01CY ATTN CA ARTHUR H. GUENTHER
  01CY ATTN NTYCE 1LT. G. KRAJEI

AFTAC
PATRICK AFB, FL 32925
  01CY ATTN TN

AIR FORCE AVIONICS LABORATORY
WRIGHT-PATTERSON AFB, OH 45433
  01CY ATTN AAD WADE HUNT
  01CY ATTN AAD ALLEN JOHNSON

DIRECTOR
STRATEGIC SYSTEMS PROJECT OFFICE
DEPARTMENT OF THE NAVY
WASHINGTON, DC 20376
  01CY ATTN NSP-2141
  01CY ATTN NSSP-2722 FRED WIMBERLY

COMMANDER
NAVAL SURFACE WEAPONS CENTER
DAHLGREN LABORATORY
DAHLGREN, VA 22448
  01CY ATTN CODE DF-14 R. BUTLER

OFFICER OF NAVAL RESEARCH
ARLINGTON, VA 22217
  01CY ATTN CODE 465
  01CY ATTN CODE 461
  01CY ATTN CODE 402
  01CY ATTN CODE 420
  01CY ATTN CODE 421

COMMANDER
FOREIGN TECHNOLOGY DIVISION, AFSC
WRIGHT-PATTERSON AFB, OH 45433
  01CY ATTN NICD LIBRARY
  01CY ATTN ETDP B. BALLARD

COMMANDER
ROME AIR DEVELOPMENT CENTER, AFSC
GRIFFISS AFB, NY 13441
  01CY ATTN DOC LIBRARY/TSLD
  01CY ATTN OCSE V. COYNE

STRATEGIC AIR COMMAND/XPFS
OFFUTT AFB, NB 68113
  01CY ATTN XPFS

SAMSO/SK
P.O. BOX 92960
WORLDWAY POSTAL CENTER
LOS ANGELES, CA 90009
  01CY ATTN SKA (SPACE COMM SYSTEMS) M. CLAVIN

SAMSO/MN
NORTON AFB, CA 92409
(MINUTEMAN)
  01CY ATTN MNNL

COMMANDER
ROME AIR DEVELOPMENT CENTER, AFSC
HANSCOM AFB, MA 01731
  01CY ATTN EEP A. LORENTZEN

DEPARTMENT OF ENERGY
LIBRARY ROOM G-042
WASHINGTON, DC 20545
  01CY ATTN DOC CON FOR A. LABOWITZ

DEPARTMENT OF ENERGY
ALBUQUERQUE OPERATIONS OFFICE
P.O. BOX 5400
ALBUQUERQUE, NM 87115
  01CY ATTN DOC CON FOR D. SHERWOOD

EG&G, INC.
LOS ALAMOS DIVISION
P.O. BOX 809
LOS ALAMOS, NM 85544
  01CY ATTN DOC CON FOR J. BREEDLOVE

DEPUTY CHIEF OF STAFF
RESEARCH, DEVELOPMENT, & ACQ
DEPARTMENT OF THE AIR FORCE
WASHINGTON, DC 20330
  01CY ATTN AFRDQ

HEADQUARTERS
ELECTRONIC SYSTEMS DIVISION
DEPARTMENT OF THE AIR FORCE
HANSCOM AFB, MA 01731-5000
  01CY ATTN J. DEAS ESD/SCD-4

UNIVERSITY OF CALIFORNIA
LAWRENCE LIVERMORE LABORATORY
P.O. BOX 808
LIVERMORE, CA 94550
  01CY ATTN DOC CON FOR TECH INFO DEPT
  01CY ATTN DOC CON FOR L-389 R. OTT
  01CY ATTN DOC CON FOR L-31 R. HAGER

LOS ALAMOS NATIONAL LABORATORY
P.O. BOX 1663
LOS ALAMOS, NM 87545
  01CY ATTN DOC CON FOR J. WOLCOTT
  01CY ATTN DOC CON FOR R.F. TASCHEK
  01CY ATTN DOC CON FOR E. JONES
  01CY ATTN DOC CON FOR J. MALIK
  01CY ATTN DOC CON FOR R. JEFFRIES
  01CY ATTN DOC CON FOR J. ZINN
  01CY ATTN DOC CON FOR D. WESTERVELT
  01CY ATTN D. SAPPENFIELD

LOS ALAMOS NATIONAL LABORATORY
MS D438
LOS ALAMOS, NM 87545
  01CY ATTN S.P. GARY
  01CY ATTN J. BOROVSKY

SANDIA LABORATORIES
P.O. BOX 5800
ALBUQUERQUE, NM 87115
  01CY. ATTN DOC CON FOR W. BROWN
  01CY ATTN DOC CON FOR A. THORNBROUGH
  01CY ATTN DOC CON FOR T. WRIGHT
  01CY ATTN DOC CON FOR D. DAHLGREN
  01CY ATTN DOC CON FOR 3141
  01CY ATTN DOC CON FOR SPACE PROJECT DIV

SANDIA LABORATORIES
LIVERMORE LABORATORY
P.O. BOX 969
LIVERMORE, CA 94550
  01CY ATTN DOC CON FOR B. MURPHEY
  01CY ATTN DOC CON FOR T. COOK

OFFICE OF MILITARY APPLICATION
DEPARTMENT OF ENERGY
WASHINGTON, DC 20545
  01CY ATTN DOC CON DR. YO SONG

NATIONAL OCEANIC & ATMOSPHERIC ADMIN
ENVIRONMENTAL RESEARCH LABORATORIES
DEPARTMENT OF COMMERCE
BOULDER, CO 80302
  01CY ATTN R. GRUBB

DEPARTMENT OF DEFENSE CONTRACTORS

AEROSPACE CORPORATION
P.O. BOX 92957
LOS ANGELES, CA 90009
01CY ATTN I. GARFUNKEL
01CY ATTN T. SALMI
01CY ATTN V. JOSEPHSON
01CY ATTN S. BOWER
01CY ATTN D. OLSEN

ANALYTICAL SYSTEMS ENGINEERING CORP
5 OLD CONCORD ROAD
BURLINGTON, MA 01803
01CY ATTN RADIO SCIENCES

AUSTIN RESEARCH ASSOC., INC.
1901 RUTLAND DRIVE
AUSTIN, TX 78758
01CY ATTN L. SLOAN
01CY ATTN R. THOMPSON

BERKELEY RESEARCH ASSOCIATES, INC.
P.O. BOX 983
BERKELEY, CA 94701
01CY ATTN J. WORKMAN
01CY ATTN C. PRETTIE
01CY ATTN S. BRECHT

BOEING COMPANY, THE
P.O. BOX 3707
SEATTLE, WA 98124
01CY ATTN G. KEISTER
01CY ATTN D. MURRAY
01CY ATTN G. HALL
01CY ATTN J. KENNEY

CHARLES STARK DRAPER LABORATORY, INC.
555 TECHNOLOGY SQUARE
CAMBRIDGE, MA 02139
01CY ATTN D.B. COX
01CY ATTN J.P. GILMORE

GTE SYLVANIA, INC.
ELECTRONICS SYSTEMS GRP-EASTERN DIV
77 A STREET
NEEDHAM, MA 02194
01CY ATTN DICK STEINHOF

HSS, INC.
2 ALFRED CIRCLE
BEDFORD, MA 01730
01CY ATTN DONALD HANSEN

ILLINOIS, UNIVERSITY OF
107 COBLE HALL
150 DAVENPORT HOUSE
CHAMPAIGN, IL 61820
(ALL CORRES ATTN DAN MCCLELLAND)
01CY ATTN K. YEH

INSTITUTE FOR DEFENSE ANALYSES
1801 NO. BEAUREGARD STREET
ALEXANDRIA, VA 22311
01CY ATTN J.M. AEIN
01CY ATTN ERNEST BAUER
01CY ATTN HANS WOLFARD
01CY ATTN JOEL BENGSTON

COMSAT LABORATORIES
22300 COMSAT DRIVE
CLARKSBURG, MD 20871
01CY ATTN G. HYDE

CORNELL UNIVERSITY
DEPARTMENT OF ELECTRICAL ENGINEERING
ITHACA, NY 14850
01CY ATTN D.T. FARLEY, JR.

ELECTROSPACE SYSTEMS, INC.
BOX 1359
RICHARDSON, TX 75080
01CY ATTN H. LOGSTON
01CY ATTN SECURITY (PAUL PHILLIPS)

EOS TECHNOLOGIES, INC.
606 Wilshire Blvd.
Santa Monica, CA 90401
01CY ATTN C.B. GABBARD
01CY ATTN R. LELEVIER

ESL, INC.
495 JAVA DRIVE
SUNNYVALE, CA 94086
01CY ATTN J. ROBERTS
01CY ATTN JAMES MARSHALL

GENERAL ELECTRIC COMPANY
SPACE DIVISION
VALLEY FORGE SPACE CENTER
GODDARD BLVD KING OF PRUSSIA
P.O. BOX 8555
PHILADELPHIA, PA 19101
01CY ATTN M.H. BORTNER
SPACE SCI LAB

GENERAL ELECTRIC TECH SERVICES
CO., INC.
HMES
COURT STREET
SYRACUSE, NY 13201
01CY ATTN G. MILLMAN

GEOPHYSICAL INSTITUTE
UNIVERSITY OF ALASKA
FAIRBANKS, AK 99701
(ALL CLASS ATTN: SECURITY OFFICER)
01CY ATTN T.N. DAVIS (UNCLASS ONLY)
01CY ATTN NEAL BROWN (UNCLASS ONLY)

KAMAN TEMPO-CENTER FOR ADVANCED
STUDIES
816 STATE STREET (P.O DRAWER QQ)
SANTA BARBARA, CA 93102
01CY ATTN DASIAC
01CY ATTN WARREN S. KNAPP
01CY ATTN WILLIAM MCNAMARA
01CY ATTN B. GAMBILL

LINKABIT CORP
10453 ROSELLE
SAN DIEGO, CA 92121
01CY ATTN IRWIN JACOBS

LOCKHEED MISSILES & SPACE CO., INC
P.O. BOX 504
SUNNYVALE, CA 94088
01CY ATTN DEPT 60-12
01CY ATTN D.R. CHURCHILL

INTL TEL & TELEGRAPH CORPORATION
500 WASHINGTON AVENUE
NUTLEY, NJ 07110
01CY ATTN TECHNICAL LIBRARY

JAYCOR
11011 TORREYANA ROAD
P.O. BOX 85154
SAN DIEGO, CA 92138
01CY ATTN J.L. SPERLING

JOHNS HOPKINS UNIVERSITY
APPLIED PHYSICS LABORATORY
JOHNS HOPKINS ROAD
LAUREL, MD 20810
01CY ATTN DOCUMENT LIBRARIAN
01CY ATTN THOMAS POTEMRA
01CY ATTN JOHN DASSOULAS

KAMAN SCIENCES CORP
P.O. BOX 7463
COLORADO SPRINGS, CO 80933
01CY ATTN T. MEAGHER

MISSION RESEARCH CORPORATION
735 STATE STREET
SANTA BARBARA, CA 93101
01CY ATTN P. FISCHER
01CY ATTN W.F. CREVIER
01CY ATTN STEVEN L. GUTSCHE
01CY ATTN R. BOGUSCH
01CY ATTN R. HENDRICK
01CY ATTN RALPH KILB
01CY ATTN DAVE SOWLE
01CY ATTN F. FAJEN
01CY ATTN M. SCHEIBE
01CY ATTN CONRAD L. LONGMIRE
01CY ATTN B. WHITE
01CY ATTN R. STAGAT

MISSION RESEARCH CORP.
1720 RANDOLPH ROAD, S.E.
ALBUQUERQUE, NM 87106
01CY R. STELLINGWERF
01CY M. ALME
01CY L. WRIGHT

MITRE CORP
WESTGATE RESEARCH PARK
1820 DOLLY MADISON BLVD
MCLEAN, VA 22101
01CY ATTN W. HALL
01CY ATTN W. FOSTER

PACIFIC-SIERRA RESEARCH CORP
12340 SANTA MONICA BLVD.
LOS ANGELES, CA 90025
01CY ATTN E.C. FIELD, JR.

PENNSYLVANIA STATE UNIVERSITY
IONOSPHERE RESEARCH LAB
318 ELECTRICAL ENGINEERING EAST
UNIVERSITY PARK, PA 16802
(NO CLASS TO THIS ADDRESS)
01CY ATTN IONOSPHERIC RESEARCH LAB

PHOTOMETRICS, INC.
4 ARROW DRIVE
WOBURN, MA 01801
01CY ATTN IRVING L. KOFSKY

LOCKHEED MISSILES & SPACE CO., INC.
3251 HANOVER STREET
PALO ALTO, CA 94304
01CY ATTN MARTIN WALT DEPT 52-12
01CY ATTN W.L. IMHOF DEPT 52-12
01CY ATTN RICHARD G. JOHNSON DEPT 52-12
01CY ATTN J.B. CLADIS DEPT 52-12

MARTIN MARIETTA CORP
ORLANDO DIVISION
P.O. BOX 5837
ORLANDO, FL 32805
01CY ATTN R. HEFFNER

MCDONNEL DOUGLAS CORPORATION
5301 BOLSA AVENUE
HUNTINGTON BEACH, CA 92647
01CY ATTN N. HARRIS
01CY ATTN J. MOULE
01CY ATTN GEORGE MROZ
01CY ATTN W. OLSON
01CY ATTN R.W. HALPRIN
01CY ATTN TECHNICAL LIBRARY SERVICES

PHYSICAL DYNAMICS, INC.
P.O. BOX 3027
BELLEVUE, WA 98009
01CY ATTN E.J. FREMOUW

PHYSICAL DYNAMICS, INC.
P.O. BOX 10367
OAKLAND, CA 94610
ATTN A. THOMSON

R & D ASSOCIATES
P.O. BOX 9695
MARINA DEL REY, CA 90291
01CY ATTN FORREST GILMORE
01CY ATTN WILLIAM B. WRIGHT, JR.
01CY ATTN WILLIAM J. KARZAS
01CY ATTN H. ORY
01CY ATTN C. MACDONALD

RAYTHEON CO.
528 BOSTON POST ROAD
SUDBURY, MA 01776
01CY ATTN BARBARA ADAMS

RIVERSIDE RESEARCH INSTITUTE
330 WEST 42nd STREET
NEW YORK, NY 10036
01CY ATTN VINCE TRAPANI

SCIENCE APPLICATIONS INTERNATIONAL INCORPORATED
1150 PROSPECT PLAZA
LA JOLLA, CA 92037
01CY ATTN LEWIS M. LINSON
01CY ATTN DANIEL A. HAMLIN
01CY ATTN E. FRIEMAN
01CY ATTN E.A. STRAKER
01CY ATTN CURTIS A. SMITH

SCIENCE APPLICATIONS INTERNATIONAL CORPORATION
1710 GOODRIDGE DR.
MCLEAN, VA 22102
01CY J. COCKAYNE
01CY E. HYMAN

SRI INTERNATIONAL
333 RAVENSWOOD AVENUE
MENLO PARK, CA 94025
  01CY ATTN J. CASPER
  01CY ATTN DONALD NEILSON
  01CY ATTN ALAN BURNS
  01CY ATTN G. SMITH
  01CY ATTN R. TSUNODA
  01CY ATTN DAVID A. JOHNSON
  01CY ATTN WALTER G. CHESNUT
  01CY ATTN CHARLES L. RINO
  01CY ATTN WALTER JAYE
  01CY ATTN J. VICKREY
  01CY ATTN RAY L. LEADABRAND
  01CY ATTN G. CARPENTER
  01CY ATTN G. PRICE
  01CY ATTN R. LIVINGSTON
  01CY ATTN V. GONZALES
  01CY ATTN D. MCDANIEL

TECHNOLOGY INTERNATIONAL CORP
75 WIGGINS AVENUE
BEDFORD, MA 01730
  01CY ATTN W.P. BOQUIST

TRW DEFENSE & SPACE SYS GROUP
ONE SPACE PARK
REDONDO BEACH, CA 90278
  01CY ATTN R. K. PLEBUCH
  01CY ATTN S. ALTSCHULER
  01CY ATTN D. DEE
  01CY ATTN D/ STOCKWELL
        SNTF/1575

VISIDYNE
SOUTH BEDFORD STREET
BURLINGTON, MA 01803
  01CY ATTN W. REIDY
  01CY ATTN J. CARPENTER
  01CY ATTN C. HUMPHREY

UNIVERSITY OF PITTSBURGH
PITTSBURGH, PA 15213
  01CY ATTN: N. ZABUSKY

PLEASE DISTRIBUTE ONE COPY TO EACH OF THE FOLLOWING PEOPLE (UNLESS OTHERWISE NOTED)

NAVAL RESEARCH LABORATORY
WASHINGTON, DC 20375
DR. H. GURSKY - CODE 4100
DR. J.M. GOODMAN - CODE 4180
DR. P. RODRIGUEZ - CODE 4750
DR. P. MANGE - CODE 4101
DR. R. MEIER - CODE 4140
CODE 2628 (22 COPIES)
CODE 1220

A.F. GEOPHYSICS LABORATORY
L.G. HANSCOM FIELD
BEDFORD, MA 01731
DR. T. ELKINS
DR. W. SWIDER
MRS. R. SAGALYN
DR. J.M. FORBES
DR. T.J. KENESHEA
DR. W. BURKE
DR. H. CARLSON
DR. J. JASPERSE
Dr. F.J. RICH
DR. N. MAYNARD
DR. D.N. ANDERSON

BOSTON UNIVERSITY
DEPARTMENT OF ASTRONOMY
BOSTON, MA 02215
DR. J. AARONS
DR. M. MENDILLO

CORNELL UNIVERSITY
ITHACA, NY 14850
DR. B. FEJER
DR. R. SUDAN
DR. D. FARLEY
DR. M. KELLEY

HARVARD UNIVERSITY
HARVARD SQUARE
CAMBRIDGE, MA 02138
DR. M.B. McELROY

INSTITUTE FOR DEFENSE ANALYSIS
1801 N. BEAUREGARD STREET
ARLINGTON, VA 22311
DR. E. BAUER

MASSACHUSETTS INSTITUTE OF TECHNOLOGY
PLASMA FUSION CENTER
CAMBRIDGE, MA 02139
LIBRARY, NW16-262
DR. T. CHANG
DR. R. LINDZEN

NASA
GODDARD SPACE FLIGHT CENTER
GREENBELT, MD 20771
DR. N. MAYNARD (CODE 696)
DR. R.F. BENSON
DR. K. MAEDA
Dr. S. CURTIS
Dr. M. DUBIN

COMMANDER
NAVAL AIR SYSTEMS COMMAND
DEPARTMENT OF THE NAVY
WASHINGTON, DC 20360
DR. T. CZUBA

COMMANDER
NAVAL OCEAN SYSTEMS CENTER
SAN DIEGO. CA 92152
MR. R. ROSE - CODE 5321

NOAA
DIRECTOR OF SPACE AND ENVIRONMENTAL LABORATORY
BOULDER, CO 80302
DR. A. GLENN JEAN
DR. G.W. ADAMS
DR. K. DAVIES
DR. R. F. DONNELLY

OFFICE OF NAVAL RESEARCH
800 NORTH QUINCY STREET
ARLINGTON, VA 22217
DR. G. JOINER

LABORATORY FOR PLASMA AND FUSION ENERGIES STUDIES
UNIVERSITY OF MARYLAND
COLLEGE PARK, MD 20742
JHAN VARYAN HELLMAN, REFERENCE LIBRARIAN

PENNSYLVANIA STATE UNIVERSITY
UNIVERSITY PARK, PA 16802
DR. J.S. NISBET
DR. P.R. ROHRBAUGH
DR. L.A. CARPENTER
DR. M. LEE
DR. R. DIVANY
DR. P. BENNETT
DR. E. KLEVANS

PRINCETON UNIVERSITY
PLASMA PHYSICS LABORATORY
PRINCETON, NJ 08540
DR. F. PERKINS

SAIC
1150 PROSPECT PLAZA
LA JOLLA, CA 92037
DR. D.A. HAMLIN
DR. L. LINSON
DR. E. FRIEMAN

SRI INTERNATIONAL
333 RAVENSWOOD AVENUE
MENLO PARK, CA 94025
DR. R. TSUNODA
DR. WALTER G. CHESNUT
DR. CHARLES L. RINO
DR. J. VICKREY
DR. R. LIVINGSTON

STANFORD UNIVERSITY
STANFORD, CA 94305
DR. P.M. BANKS
DR. R. HELLIWELL

U.S. ARMY ABERDEEN RESEARCH
AND DEVELOPMENT CENTER
BALLISTIC RESEARCH LABORATORY
ABERDEEN, MD
DR. J. HEIMERL

GEOPHYSICAL INSTITUTE
UNIVERSITY OF ALASKA
FAIRBANKS, AK 99701
DR. L.C. LEE

UNIVERSITY OF CALIFORNIA
LOS ALAMOS NATIONAL LABORATORY
J-10, MS-664
LOS ALAMOS, NM 87545
DR. M. PONGRATZ
DR. D. SIMONS
DR. G. BARASCH
DR. L. DUNCAN
DR. P. BERNHARDT
DR. S.P. GARY

UNIVERSITY OF ILLINOIS
DEPT. OF ELECTRICAL ENGINEERING
1406 W. GREEN STREET
URBANA, IL 61801
DR. ERHAN KUDEKI

UNIVERSITY OF CALIFORNIA,
LOS ANGELES
405 HILLGARD AVENUE
LOS ANGELES, CA 90024
DR. F.V. CORONITI
DR. C. KENNEL
DR. A.Y. WONG

UNIVERSITY OF MARYLAND
COLLEGE PARK, MD 20740
DR. K. PAPADOPOULOS
DR. E. OTT

JOHNS HOPKINS UNIVERSITY
APPLIED PHYSICS LABORATORY
JOHNS HOPKINS ROAD
LAUREL, MD 20810
DR. R. GREENWALD
DR. C. MENG
DR. T. POTEMRA

UNIVERSITY OF PITTSBURGH
PITTSBURGH, PA 15213
DR. N. ZABUSKY
DR. M. BIONDI
DR. E. OVERMAN

UNIVERSITY OF TEXAS
AT DALLAS
CENTER FOR SPACE SCIENCES
P.O. BOX 688
RICHARDSON, TX 75080
DR. R. HEELIS
DR. W. HANSON
DR. J.P. McCLURE

UTAH STATE UNIVERSITY
4TH AND 8TH STREETS
LOGAN, UT 84322
DR. R. HARRIS
DR. K. BAKER
DR. R. SCHUNK
DR. J. ST.-MAURICE
DR. N. SINGH

DIRECTOR OF RESEARCH
U.S. NAVAL ACADEMY
ANNAPOLIS, MD 21402
(2 COPIES)

IONOSPHERIC MODELING DISTRIBUTION LIST
(UNCLASSIFIED ONLY)

PLEASE DISTRIBUTE ONE COPY TO EACH OF THE FOLLOWING PEOPLE (UNLESS OTHERWISE NOTED)

NAVAL RESEARCH LABORATORY
WASHINGTON, DC 20375
DR. H. GURSKY - CODE 4100
DR. J.M. GOODMAN - CODE 4180
DR. P. RODRIGUEZ - CODE 4750
DR. P. MANGE - CODE 4101
DR. R. MEIER - CODE 4140
CODE 2628 (22 COPIES)
CODE 1220

A.F. GEOPHYSICS LABORATORY
L.G. HANSCOM FIELD
BEDFORD, MA 01731
DR. T. ELKINS
DR. W. SWIDER
MRS. R. SAGALYN
DR. J.M. FORBES
DR. T.J. KENESHEA
DR. W. BURKE
DR. H. CARLSON
DR. J. JASPERSE
Dr. F.J. RICH
DR. N. MAYNARD
DR. D.N. ANDERSON

BOSTON UNIVERSITY
DEPARTMENT OF ASTRONOMY
BOSTON, MA 02215
DR. J. AARONS
DR. M. MENDILLO

CORNELL UNIVERSITY
ITHACA, NY 14850
DR. B. FEJER
DR. R. SUDAN
DR. D. FARLEY
DR. M. KELLEY

HARVARD UNIVERSITY
HARVARD SQUARE
CAMBRIDGE, MA 02138
DR. M.B. McELROY

INSTITUTE FOR DEFENSE ANALYSIS
1801 N. BEAUREGARD STREET
ARLINGTON, VA 22311
DR. E. BAUER

MASSACHUSETTS INSTITUTE OF TECHNOLOGY
PLASMA FUSION CENTER
CAMBRIDGE, MA 02139
LIBRARY, NW16-262
DR. T. CHANG
DR. R. LINDZEN

NASA
GODDARD SPACF FLIGHT CENTER
GREENBELT, MD 20771
DR. N. MAYNARD (CODE 696)
DR. R.F. BENSON
DR. K. MAEDA
Dr. S. CURTIS
Dr. M. DUBIN

COMMANDER
NAVAL AIR SYSTEMS COMMAND
DEPARTMENT OF THE NAVY
WASHINGTON, DC 20360
DR. T. CZUBA

COMMANDER
NAVAL OCEAN SYSTEMS CENTER
SAN DIEGO. CA 92152
MR. R. ROSE - CODE 5321

NOAA
DIRECTOR OF SPACE AND ENVIRONMENTAL LABORATORY
BOULDER, CO 80302
DR. A. GLENN JEAN
DR. G.W. ADAMS
DR. K. DAVIES
DR. R. F. DONNELLY

OFFICE OF NAVAL RESEARCH
800 NORTH QUINCY STREET
ARLINGTON, VA 22217
DR. G. JOINER

LABORATORY FOR PLASMA AND FUSION ENERGIES STUDIES
UNIVERSITY OF MARYLAND
COLLEGE PARK, MD 20742
JHAN VARYAN HELLMAN, REFERENCE LIBRARIAN

PENNSYLVANIA STATE UNIVERSITY
UNIVERSITY PARK, PA 16802
DR. J.S. NISBET
DR. P.R. ROHRBAUGH
DR. L.A. CARPENTER
DR. M. LEE
DR. R. DIVANY
DR. P. BENNETT
DR. E. KLEVANS

PRINCETON UNIVERSITY
PLASMA PHYSICS LABORATORY
PRINCETON, NJ 08540
DR. F. PERKINS

SAIC
1150 PROSPECT PLAZA
LA JOLLA, CA 92037
DR. D.A. HAMLIN
DR. L. LINSON
DR. E. FRIEMAN

SRI INTERNATIONAL
333 RAVENSWOOD AVENUE
MENLO PARK, CA 94025
DR. R. TSUNODA
DR. WALTER G. CHESNUT
DR. CHARLES L. RINO
DR. J. VICKREY
DR. R. LIVINGSTON

STANFORD UNIVERSITY
STANFORD, CA 94305
DR. P.M. BANKS
DR. R. HELLIWELL

U.S. ARMY ABERDEEN RESEARCH
AND DEVELOPMENT CENTER
BALLISTIC RESEARCH LABORATORY
ABERDEEN, MD
DR. J. HEIMERL

GEOPHYSICAL INSTITUTE
UNIVERSITY OF ALASKA
FAIRBANKS, AK 99701
DR. L.C. LEE

UNIVERSITY OF CALIFORNIA
LOS ALAMOS NATIONAL LABORATORY
J-10, MS-664
LOS ALAMOS, NM 87545
DR. M. PONGRATZ
DR. D. SIMONS
DR. G. BARASCH
DR. L. DUNCAN
DR. P. BERNHARDT
DR. S.P. GARY

UNIVERSITY OF ILLINOIS
DEPT. OF ELECTRICAL ENGINEERING
1406 W. GREEN STREET
URBANA, IL 61801
DR. ERHAN KUDEKI

UNIVERSITY OF CALIFORNIA,
LOS ANGELES
405 HILLGARD AVENUE
LOS ANGELES, CA 90024
DR. F.V. CORONITI
DR. C. KENNEL
DR. A.Y. WONG

UNIVERSITY OF MARYLAND
COLLEGE PARK, MD 20740
DR. K. PAPADOPOULOS
DR. E. OTT

JOHNS HOPKINS UNIVERSITY
APPLIED PHYSICS LABORATORY
JOHNS HOPKINS ROAD
LAUREL, MD 20810
DR. R. GREENWALD
DR. C. MENG
DR. T. POTEMRA

UNIVERSITY OF PITTSBURGH
PITTSBURGH, PA 15213
DR. N. ZABUSKY
DR. M. BIONDI
DR. E. OVERMAN

UNIVERSITY OF TEXAS
AT DALLAS
CENTER FOR SPACE SCIENCES
P.O. BOX 688
RICHARDSON, TX 75080
DR. R. HEELIS
DR. W. HANSON
DR. J.P. McCLURE

UTAH STATE UNIVERSITY
4TH AND 8TH STREETS
LOGAN, UT 84322
DR. R. HARRIS
DR. K. BAKER
DR. R. SCHUNK
DR. J. ST.-MAURICE
DR. N. SINGH

DIRECTOR OF RESEARCH
U.S. NAVAL ACADEMY
ANNAPOLIS, MD 21402
(2 COPIES)

END

12-86

DTIC